Dynamical aspects of isoscaling

C. O. Dorso,[1] C. R. Escudero,[2] M. Ison,[1] and J. A. López[2]
[1]*Departamento de Física, FCEN, Universidad de Buenos Aires, Núñez, Argentina*
[2]*Department of Physics, University of Texas at El Paso, El Paso, Texas 79968, USA*
(Received 11 April 2005; revised manuscript received 27 January 2006; published 3 April 2006)

The origin and dynamical evolution of isoscaling was studied using classical molecular dynamics simulations of ^{40}Ca+^{40}Ca, ^{48}Ca+^{48}Ca, and ^{52}Ca+^{52}Ca at beam energies ranging from 20 to 85 MeV/nucleon. The analysis included a study of the time evolution of this effect. Isoscaling was observed to exist at all energies in these reactions from the early primary isotope distributions (produced by systems not yet in thermal equilibrium) all the way to 5000 fm/c.

DOI: 10.1103/PhysRevC.73.044601 PACS number(s): 24.10.Lx, 02.70.Ns, 25.70.Pq, 64.70.Fx

I. INTRODUCTION

Experimental advances, that now permit the study of nuclear reactions involving radioactive isotopes, have propelled the isotopic degree of freedom to the forefront [1–5]. It is expected, for instance, that this new variable of control could shed light on charge equilibration in heavy-ion reactions and on the role played by the isotope asymmetry terms of the equation of state of nuclear matter [4].

The main tool for inspection of this new observable is based on the isotope yields of central collisions of similar, but isotopically different, reactions [1,5]. The ratio of isotope yields from reactions 1 and 2, $R_{21}(N, Z)$, has been found to depend exponentially on the isotope neutron number N and proton number Z:

$$R_{21}(N, Z) = \frac{Y_2(N, Z)}{Y_1(N, Z)} \approx e^{\alpha N+\beta Z}, \tag{1}$$

where α and β are fitting parameters. Equations of the form of Eq. (1) can be linked, under some approximations, to primary isotope yields produced by disassembling equilibrated systems in microcanonical and grand canonical ensembles [4], as well as to breakups in canonical [6] ensembles.

Little reflection is needed to understand that R_{21} could be affected by many reaction variables. Its direct dependence on the experimentally measured yields, Y_1 and Y_2, makes R_{21} vulnerable to anything that can modify the isotopic content of the initial fragment yield, be this out-of-equilibrium breakup, secondary fission of primordial fragments, light particle emission, and the like. As these effects have varying lifetimes, it is very likely that the experimentally captured yield contains an integral of all of these effects on the primary distribution. This casts a shadow of doubt on the isoscaling-related conclusions obtained by the use of microcanonical, canonical, and grand canonical breakup scenarios and calls for the use of an unconstrained model to ratify the main findings of equilibrium models.

This article aims at elucidating the origin and dynamical evolution of isoscaling using a model not restricted by assumptions such as the existence of freeze-out stages, thermal and chemical equilibration, or unrealistic volume constraints [7]. In the next section, the molecular dynamics (MD) model used is introduced along with the fragment recognition algorithm selected for this study. The fitting procedure used to extract the isoscaling exponential law [Eq. (1)] from the simulations is presented in Sec. III followed by results consisting of the observation of isoscaling at long times, its dependence on the reaction energy, the time evolution of such a law during the reaction, and its connection to thermodynamical observables. The manuscript closes with a summary of the main conclusions.

II. MOLECULAR DYNAMICS

To study the origin of isoscaling, a model capable of reproducing both the out-of-equilibrium and the equilibrium parts of a collision is needed. As statistical and other equilibrium models [8,9] lack—by construction—all relevant collision-induced correlations, a dynamical model is thus needed. Most such dynamical models, nevertheless, lack higher-order correlations and have varying difficulties in producing fragmentation [10–14]. In the present work, we use an MD model that can describe nonequilibrium dynamics, hydrodynamic flow, and changes of phase without adjustable parameters. The combination of this MD code with a fragment-recognition algorithm, has been dubbed LATINO [15], and in recent years it has been applied successfully to study, among other things, neck fragmentation [16], phase transitions [17], critical phenomena [18,19], and the caloric curve [20,21] in nuclear reactions.

The MD code uses a two-body potential composed of the Coulomb interaction plus a nuclear part [22] that correctly reproduces nucleon-nucleon cross sections, as well as the correct binding energies and densities of real nuclei. The "nuclear" part of the interaction potential is

$$\begin{aligned} V_{np}(r) &= V_r[\exp(-\mu_r r)/r - \exp(-\mu_r r_c)/r_c] \\ &\quad - V_a[\exp(-\mu_a r)/r - \exp(-\mu_a r_a)/r_a] \\ V_{nn}(r) &= V_{pp}(r) = V_0[\exp(-\mu_0 r)/r - \exp(-\mu_0 r_c)/r_c], \end{aligned} \tag{2}$$

where the cutoff radius is $r_c = 5.4$ fm, V_{np} is the potential between a neutron and a proton, and V_{nn} is that between identical nucleons. The values of the parameters of the Yukawa potentials [22] correspond to an equation of state of infinite nuclear matter with an equilibrium density of

$\rho_0 = 0.16$ fm^{-3}, a binding energy $E(\rho_0) = -16$ MeV/nucleon, and a compressibility of around 250 MeV.

To study collisions, this potential is first used along with dissipative molecular dynamics to construct "nuclei" by grouping "nucleons" at the binding energies and radii of real nuclei, and stable for times longer than the reaction time. These nuclei are then used as targets and projectiles by rotating the relative orientation of the target-nuclei combination, boosting the center-of-mass velocity of the projectile to a desired energy and leaving the target initially at rest. The trajectories of motion of individual nucleons are then calculated using the standard Verlet algorithm with an energy conservation of $\mathcal{O}(0.01\%)$.

The collision information, initially composed by the values of $(\vec{r}, \vec{p})$ of the nucleons, is then transformed into fragment information by means of a cluster-detection algorithm that, in this case, is the MSE method that was introduced decades ago [23], but was recently adapted for this field, fully analyzed, and compared with other fragment recognition algorithms [24]. According to this prescription, a particle i belongs to a cluster C if there is a particle j in C to which i is bound in the sense of $p_{ij}^2/4\mu < v_{ij}$, where p_{ij} is the relative momentum, μ the reduced mass, and v_{ij} the interparticle potential. In this cluster definition the effect of the relative momentum between the particles that form the cluster is taken into account in an approximate way; of course, at some time during the reaction, MSE yields the asymptotic cluster distribution. The resulting information contains details about the nucleon content of the emitted fragments and, as this is available at all times during the collision, it allows the study of the time evolution of quantities such as the isoscaling law.

Before we turn to a description of the analysis performed on these collisions, a word of caution is needed to underline the fact that the MD model here described is fully classical and that all quantal effects, such as the exclusion principle, Fermi motion, and isotopic content-modifying phenomena, are excluded. [The effects of Fermi motion, although formally absent, are somewhat included by the internal motion of the "nucleons" that provides "nuclei" with the proper binding energy and radius to mimic real nuclei.] Therefore, if any of the excluded effects is responsible for isoscaling, this study should not reproduce this effect. On the contrary, if isoscaling is well predicted by this classical model, this will imply that isoscaling can be explained qualitatively without assuming quantum effects.

III. ISOSCALING

The collisions ^{40}Ca+^{40}Ca, ^{48}Ca+^{48}Ca, and ^{52}Ca+^{52}Ca, were studied at beam energies of 20, 25, 35, 45, 65, and 85 MeV/nucleon with 2000 collisions performed at each energy. Data from these collisions were used to construct the corresponding yield matrices $Y_i(N, Z)$, where i stands for the reaction, and N and Z for the neutron and proton numbers, respectively. These matrices were then used to calculate the ratio $R_{21}(N, Z) = Y_2(N, Z)/Y_1(N, Z)$ for the combinations of reactions ^{40}Ca with ^{48}Ca, ^{40}Ca with ^{52}Ca, and ^{48}Ca with ^{52}Ca at each of the energy values. These ratios were calculated at different reaction times starting at impact ($t = 0$) and ending at 5000 fm/c. Fits to the isoscaling exponential law [Eq. (1)] were obtained using a standard least-squares method for all points corresponding to each reaction and energy, a procedure that yielded values of the parameters α and β for each of the calculated times. Next, studies of the energy dependence of isoscaling at long times and its behavior during the dense part of the reaction are presented.

A. Isoscaling at long times

Experimental results always correspond to asymptotic values, taking into account that, at the energies listed below, the time needed for an unobstructed projectile to cross the length of the target is of the order of a few fm/c, it is safe to consider times of, say, 1000 fm/c close to the asymptotic values; in this study, nevertheless, the calculation was extended to 5 times this value.

Figure 1 shows the obtained values of $R_{21}(N, Z)$ and the corresponding fit to the isoscaling exponential law (1) for the case ^{40}Ca-^{48}Ca at 35 MeV/nucleon at 1250 fm/c. The fact that LATINO reproduces the reactions sufficiently well as to produce isoscaling at long times is obvious from this figure. Other reactions (i.e., with other masses and energies) yield similar results.

Upon applying the fitting procedures described in Sec. III for each of the three ratios of reactions, values of α and β were obtained for each of the energies. Figure 2 shows the values of these fitting parameters at times of 5000 fm/c as a function of beam energy per nucleon for the ratios of the reactions ^{40}Ca-^{48}Ca, ^{40}Ca-^{52}Ca, and ^{48}Ca-^{52}Ca. The smooth trends of α and β are in the range of values obtained by other investigators [4,5,14,25,26].

It is instructive to compare these results to those recently obtained using quantal molecular dynamics simulations with the AMD-V model [14]. In that work, collisions between ^{40}Ca+^{40}Ca, ^{48}Ca+^{48}Ca, and ^{60}Ca+^{60}Ca at 35 MeV/nucleon were performed, and an isoscaling-looking behavior was observed for their R_{21}. The power-law fit obtained for the ratio

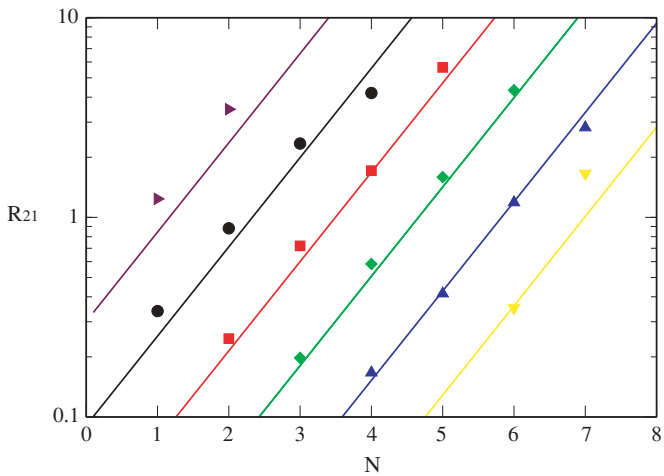

FIG. 1. (Color online) Long time behavior of isoscaling. Typical fit to $R_{21}(N, Z)$ for the case ^{40}Ca-^{48}Ca at 35 MeV/nucleon at 1250 fm/c.

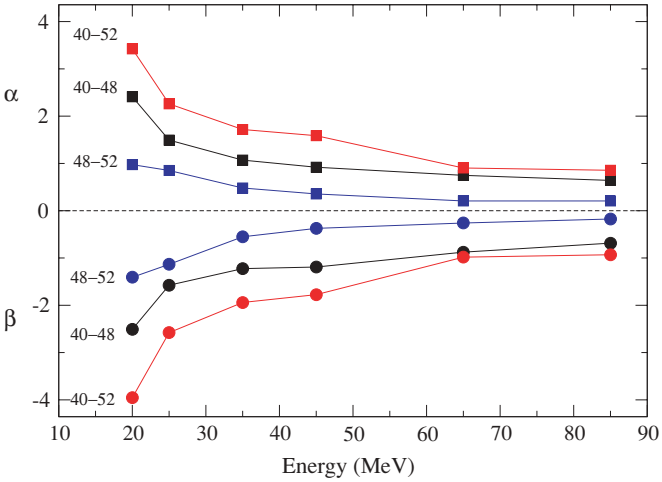

FIG. 2. (Color online) Energy dependence of fitting parameters α and β for three reactions ^{40}Ca+^{40}Ca, ^{48}Ca+^{48}Ca, and ^{52}Ca+^{52}Ca, at beam energies ranging from 20 to 85 MeV/nucleon and at $t =$ 5000 fm/c.

of ^{48}Ca +^{48} Ca to of ^{40}Ca +^{40} Ca yielded an $\alpha = 1.03$ and $\beta = 1.22$. These values agree with the results here obtained for a similar case: $\alpha = 1.07$ and $\beta = 1.22$ (cf. Fig. 2); other AMD-V results are also in line with our classical MD simulations.

As stated before, because this study is based on a classical MD model, the fact that isoscaling is well reproduced by it implies that it can be explained qualitatively without assuming quantum effects that could modify the isotopic content of the fragments. To gain a deeper insight into the origin of isoscaling, we now turn to a study to its time evolution during the reaction.

B. Evolution of isoscaling

As the nucleon information is available throughout the reaction, the yields and, thus, the ratio R_{21} can be calculated at any time during the collision. Figure 3 shows early (at

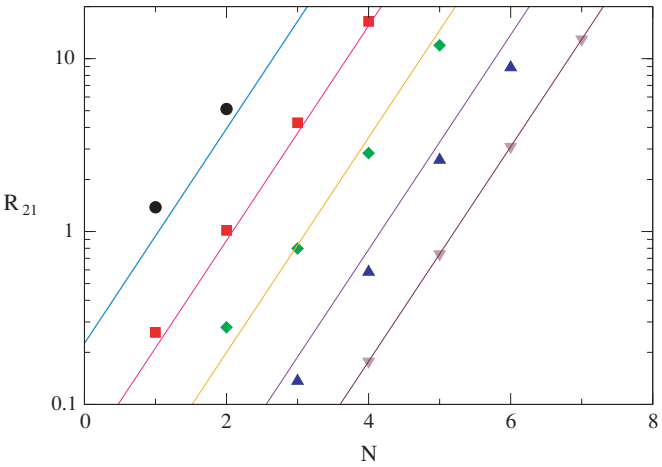

FIG. 3. (Color online) Early behavior of isoscaling. Typical fit to $R_{21}(N, Z)$ for the case ^{40}Ca-^{48}Ca at 35 MeV/nucleon at 125 fm/c.

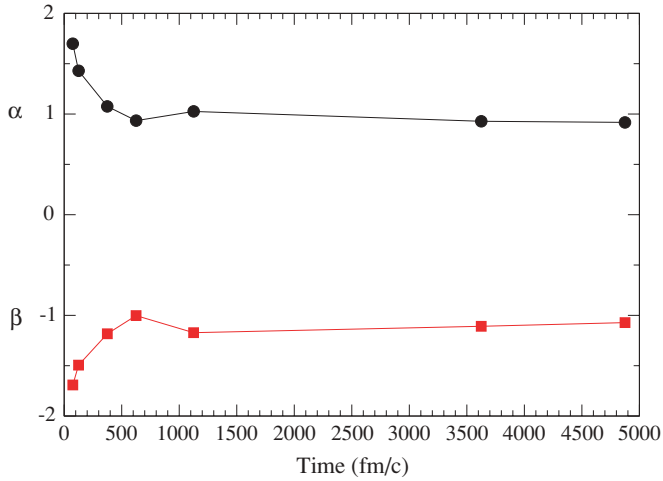

FIG. 4. (Color online) Time evolution of α and β for the case ^{40}Ca-^{48}Ca at 35 MeV/nucleon.

125 fm/c) values of $R_{21}(N, Z)$ and the corresponding fit to the isoscaling exponential law [Eq. (1)], for the case ^{40}Ca-^{48}Ca at 35 MeV/nucleon. The observed goodness of the isoscaling exponential law appears to be as good in early times as at long times. Other reactions yield similar results.

Repeating the fitting procedure described in Sec. III, it is possible to obtain values of α and β at different times. Figure 4 shows the time evolution of α and β obtained from the ratio of yields of ^{40}Ca-^{48}Ca at 35 MeV/nucleon as a function of reaction time.

As attested by Fig. 3 and with varying values of α and β (cf. Fig. 4), isoscaling appears to be present in the reaction from early times. This, in agreement with the findings of [4], rules out long-time effects, such as secondary decays, as the cause of isoscaling. Thus, our search for the origin of this effect should now be directed to earlier times of the reaction, those in which the system is still rather dense and highly interacting.

C. Isoscaling and dynamics

As outlined in Ref. [1], the parameters α and β of the power law [Eq. (1)], can be linked to the differences between the neutron and proton separation energies for the two reactions. Assuming that the reactions populate a grand canonical ensemble, and that the secondary decays have little impact on the resulting R_{21}, it can be shown that $\alpha = (\mu_{n2} - \mu_{n1})/T$ and $\beta = (\mu_{p2} - \mu_{p1})/T$, where μ_{ni} and μ_{pi} are the neutron and proton chemical potentials of reaction i and T is the equilibrium temperature of the reaction, assumed to be the same for both reactions of the isoscaling comparison.

The main assumption of the preceding arguments, namely the existence of thermodynamic equilibrium, is questionable in systems that are finite, expanding, and disassembling. Added to this concern, of course, is the assumption of a common temperature in both reactions, as well as unique separation energies throughout the disassembling systems. Although these assumptions are difficult to verify, in this section we make an attempt to better understand these premises.

1. Thermal equilibrium

As the temperature of a fragmenting system is not well defined, we first focus only on the dynamical properties of the largest fragment; to have an approximate view of the thermalization process, in the spirit of Ref. [27], we define two effective temperatures. Using cylindrical coordinates and decomposing the system in the beam axis (z) and in the reaction plane (xy), it is possible to calculate the collective expansion velocity by

$$v_{\rm beam}(t) = \left\langle \frac{1}{N_{BF}} \sum_{i=1}^{N_{BF}} \frac{\mathbf{v}^{(i)}(t) \cdot \mathbf{z}^{(i)}(t)}{|\mathbf{z}^{(i)}(t)|} \right\rangle_e , \qquad (3)$$

in the beam axis direction and

$$v_{\rm perp}(t) = \left\langle \frac{1}{N_{BF}} \sum_{i=1}^{N_{BF}} \mathbf{v}^{(i)}(t) \cdot \hat{r}^{(i)}(t) \right\rangle_e , \qquad (4)$$

in the reaction (perpendicular) plane. Here N_{BF} is the number of particles in the biggest source and $\langle\,\rangle_e$ denotes an ensemble average. All quantities are calculated in the center of mass of the biggest emitting source.

With these velocities, effective temperatures can be defined in terms of the velocity fluctuations:

$$T_{\rm loc}^{\rm beam} = \left\langle \frac{2}{N_{BF}} \sum_{i=1}^{N_{BF}} \frac{m}{2} \left[\mathbf{v}_z^{(i)}(t) - v_{\rm beam}(t) \right]^2 \right\rangle_e \qquad (5)$$

and

$$T_{\rm loc}^{\rm perp} = \left\langle \frac{1}{N_{BF}} \sum_{i=1}^{N_{BF}} \frac{m}{2} \left[\mathbf{v}_r^{(i)}(t) - v_{\rm perp}(t) \right]^2 \right\rangle_e , \qquad (6)$$

where the subscript loc as been added to emphasize that these temperatures represent local, rather than global, measures. For the ease of comparison, Fig. 5 shows the time evolution of the two effective temperatures together with the time evolution of the (scaled) collective velocities and the (scaled) average size of the biggest source; see caption for details.

In this figure $t = 0$ corresponds to the time at which the two nuclei start interacting via the nuclear short-range interaction. At this time the collective expansion in the reaction plane starts to grow, reaching a maximum at $t = 35$ fm/c and finally vanishing at about $t = 185$ fm/c. However the collective motion in the beam axis first shows a compression stage, followed by an expansion, which ends at about $t = 45$ fm/c.

Regarding the effective temperatures, they both attain the same value at about $t = 45$ fm/c, time at which equilibration in the three spatial degrees of freedom can be assumed. As it will be shown in Fig. 6, the same effect occurs for ^{52}Ca + ^{52}Ca at 35 MeV/nucleon but not until 90 fm/c.

It is worthwhile noticing that this behavior of the effective temperatures takes place while the mass of the biggest fragment is quite close to the sum of projectile and target. Afterwards, the system cools down while emitting fragments. A second observation is that the maximum temperatures observed (around 4 MeV) are consistent with those derived from alternative analyses [28]; studies of other reactions at different energies also yielded similar results.

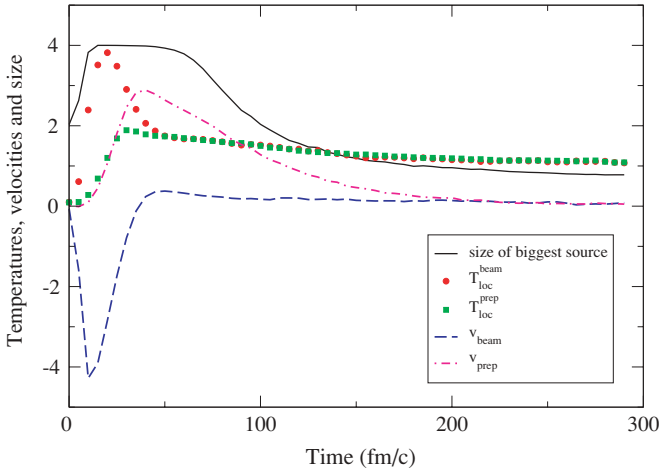

FIG. 5. (Color online) Time evolution of the effective temperatures for the reaction ^{40}Ca + ^{40}Ca at 35 MeV/nucleon. The behavior of $T_{\rm loc}^{\rm beam}$ is shown with dots, $T_{\rm loc}^{\rm perp}$ with squares, the collective velocities (in units of $c/40$) in the beam axis is shown with the dashed line, and in the reaction plane with a dot-dashed line. Also shown with a continuous line is the average size of the biggest source, scaled by a factor 1/20.

2. Thermal symmetry of isotopic reactions

An equally important point is that of the similarity of the temperatures in the two reactions included in the ratio R_{21}. To study this point we further focus on the dynamical properties of the largest fragments produced on the two collisions.

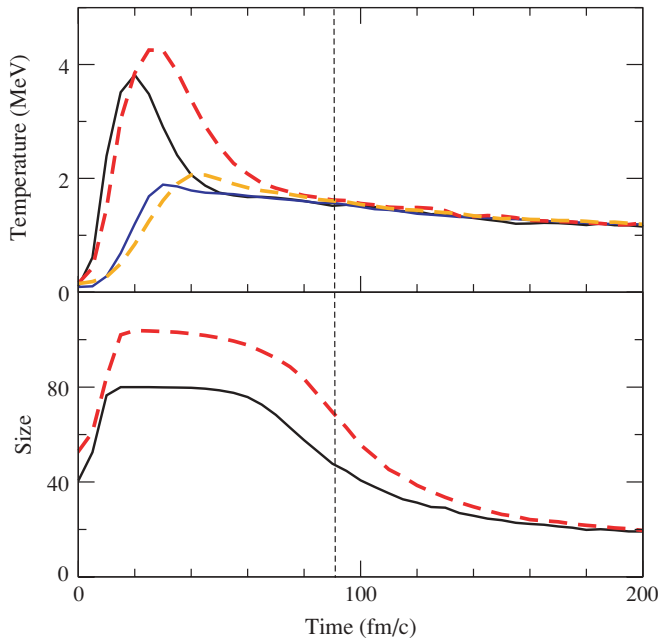

FIG. 6. (Color online) Comparison of temperatures (top panel) and sizes of largest fragments (bottom panel) obtained in the reactions ^{40}Ca+^{40}Ca (continuous lines) and ^{52}Ca+^{52}Ca (dashed lines) both at 35 MeV/nucleon. The top panel shows the time distribution of the $T_{\rm loc}^{\rm beam}$ (higher curves) and of the $T_{\rm loc}^{\rm perp}$ (lower curves). The vertical dashed line indicates the time when both reactions are in thermal equilibrium and are under conditions of thermal symmetry.

Figure 6 shows a comparison of temperatures (top panel) and sizes of largest fragments (bottom panel) obtained in the reactions $^{40}Ca + ^{40}Ca$ (solid lines) and $^{52}Ca + ^{52}Ca$ both at 35 MeV/nucleon. The top panel shows the time distribution of the temperatures T_{loc}^{beam} (higher curves) and T_{loc}^{perp} (lower curves).

Figure 6 indicates that the time evolutions of the dynamical observables of both reactions are, on average, very similar except at early times. In the beginning of the reaction, while isoscaling sets in, the largest fragments of both reactions suffer similar compressions and expansions but at different times and with very different average temperatures. The two T_{loc}^{beam}, for instance, peak at times differing by about 15 fm/c and with magnitudes different by a factor of the order of 30%. Any isoscaling observed before the convergence of all the four temperatures would be produced by systems not yet in states of thermal symmetry, which for the case of $^{52}Ca + ^{52}Ca$ compared to $^{40}Ca + ^{40}Ca$ at 35 MeV/nucleon does not take place until 90 fm/c.

Even though this difference in temperature vanishes for later times, its importance cannot be underestimated as it occurs precisely when the n to p ratios and, thus, R_{21} are being established. [The first values of α and β of Fig. 4, for instance, show that isoscaling already existed at a time of 75 fm/c.] The existence of isoscaling while the systems have not yet achieved thermal equilibrium individually nor while the corresponding temperatures of the two reactions converge with each other suggests the possibility of achieving isoscaling under conditions other than those of thermal equilibrium.

[This, in turn would cast serious doubts about the proposed relationship between α and β and the neutron and proton chemical potentials and would, indeed, lead to relationships of the type $\alpha = (\mu_{n2}/T_2 - \mu_{n1}/T_1)$ and $\beta = (\mu_{p2}/T_2 - \mu_{p1}/T_1)$. Although the existence of different source temperatures could possibly be handled [25], the dependence of μ on T [$\mu(T) - \mu(0) \propto T^2$ [29]] combined with the rapid cooling in early times, makes it difficult to argue for the existence of well-defined separation energies that could apply throughout the reaction. The same can be said about macroscopic constructs such as the symmetry energy of the medium, an important factor in the isospin dynamics in mean-field models such as QMD and IQMD. The observed variation of the temperature in turn implies a varying symmetry energy strength that, if extracted experimentally from data, would yield only an average of all the values convoluted throughout the evolution of the reaction. Put in terms of fragments and isoscaling, at best, what exists at, say, 125 fm/c is the sum of fragments emitted at earlier times that might have undergone subsequent decay, the final yield ratio R_{21} can only be said to be a product of the time integral of decays that occurred under different values of the chemical potentials or symmetry energy strengths.]

In addition to ruling out the chemical potential as the decisive factor in establishing isoscaling, the previous results introduce the need to consider the addition of decays and other nucleon-rearranging processes that take place at different times during the reaction. The importance of this factor can be quantified by inspecting the time evolution of the particle production for different types of particles.

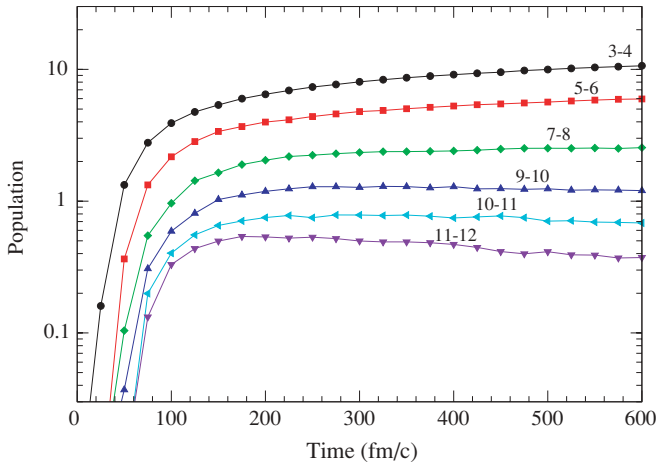

FIG. 7. (Color online) Population of different mass bins as a function of time for the reaction ^{40}Ca on ^{40}Ca at 35 MeV/nucleon. Circles (3-4), squares (5-6), etc.

Figure 7 shows the average population of different mass bins obtained at different times for the reaction ^{40}Ca on ^{40}Ca at 35 MeV/nucleon. This time chart clearly illustrates that at times smaller than 100 fm/c, the fragment mass distribution is far from reaching its final value. Furthermore, because, as seen in Fig. 3, isoscaling is already alive and well at 75 fm/c, i.e., well before the stabilization of most mass bins, the isoscaling power law observed at early times is only a work in progress produced by fragments emitted in previous times.

By induction, all values of α and β at a given time include contributions of all earlier fragments and will pass their own contribution to later values of these exponents. It does appear as if the origin of isospin is connected more to the statistical sampling induced by the collision, as observed by Ono *et al.* [14], than to specific details of the dynamics of the reaction; this will be explored further in a follow-up investigation [30].

IV. CONCLUSIONS

The origin and evolution of isoscaling was studied using classical molecular dynamics simulations combined with a fragment-recognition algorithm. Collisions of $^{40}Ca+^{40}Ca$, $^{48}Ca+^{48}Ca$, and $^{52}Ca+^{52}Ca$, at energies from 20 to 85 MeV/nucleon were used to construct the ratios $R_{21}(N, Z)$ and to obtain the fitting parameters α and β for the three possible combinations of reactions at all energies and for times from impact to 5000 fm/c.

Isoscaling was found at long times from 1250 to 5000 fm/c, the last calculated time. The fitting parameters of the R_{21} at long times showed a smooth variation with respect to the beam energy. Although excellent agreement was found with quantal molecular dynamics results, these classical results indicate that isoscaling can be explained qualitatively without assuming quantum effects.

A power law fit of R_{21} was possible from early times during the collision (cf. Fig. 4) and it was maintained, with smoothly varying values of α and β, throughout the reaction. Examining

the time evolution of the fragment mass distribution, isoscaling appears to exist before this distribution reaches its final value.

Examining this period of time it was found that individual reactions do not achieve individual thermal equilibrium before a time ranging from 50 to about 90 fm/c and do not reach a state of thermal symmetry before these equilibration times. During this time the largest fragments of both reactions undergo a compression/heating phase followed by an expansion/cooling period with average temperatures that differ by up to 30%.

In summary, we found that isoscaling exists in classical systems, power law fits to R_{21} can be obtained in dense systems out of equilibrium, it is maintained as the system reaches equilibrium, expands, and fragments. Our results seem to indicate that isoscaling, i.e., the possibility of fitting the yields ratio R_{21} by a power law, exists before the reactions achieve thermal equilibrium and thermal symmetry, which in turn breaks the one-to-one correspondence believed to exist between isoscaling and the thermodynamic conditions of the dense part of the reactions. Furthermore, the observed time variation of the α and β indicate that the final values of these parameters could be related to the last part of the reaction where the fragments finish cooling by particle evaporation. The importance on isoscaling of factors not included in this study, such as the role of geometry and sampling techniques, will be considered in our following work [30].

ACKNOWLEDGMENTS

C.O.D acknowledges the support of grant x360 from the Universidad de Buenos Aires, and grant PIP5969 from CONICET, and the hospitality of the University of Texas at El Paso where this project was initiated. The authors are indebted to A. Barrañón for facilitating the initial configurations of the "*nuclei*" used in these simulations.

[1] H. S. Xu, M. B. Tsang, T. X. Liu, X. D. Liu, W. G. Lynch, W. P. Tan, A. Vander Molen, G. Verde, A. Wagner, H. F. Xi, C. K. Gelbke, L. Beaulieu, B. Davin, Y. Larochelle, T. Lefort, R. T. de Souza, R. Yanez, V. E. Viola, R. J. Charity, and L. G. Sobotka, Phys. Rev. Lett. **85**, 716 (2000).
[2] H. Johnston *et al*., Phys. Lett. **B3715**, 186 (1996).
[3] R. Laforest *et al*., Phys. Rev. C **59**, 2567 (1999).
[4] M. B. Tsang, C. K. Gelbke, X. D. Liu, W. G. Lynch, W. P. Tan, G. Verde, H. S. Xu, W. A. Friedman, R. Donangelo, S. R. Souza, C. B. Das, S. Das Gupta, and D. Zhabinsky, Phys. Rev. C **64**, 054615 (2001).
[5] M. B. Tsang, W. A. Friedman, C. K. Gelbke, W. G. Lynch, G. Verde, and H. Xu, Phys. Rev. Lett. **86**, 5023 (2001).
[6] C. B. Das, S. Das Gupta, X. D. Liu, and M. B. Tsang, Phys. Rev. C **64**, 044608 (2001).
[7] T. Furuta and A. Ono, arXiv:nucl-th/0305050 **V2**, (2003) (submitted to PRC).
[8] J. P. Bondorf, A. S. Botvina, A. S. Iljinov, l. N. Mishustin, and K. Sneppen, Phys. Rep. **257**, 133 (1995).
[9] W. A. Friedman, Phys. Rev. Lett. **60**, 2125 (1988); Phys. Rev. C **42**, 667 (1990).
[10] G. F. Bertsch and S. Das Gupta, Phys. Rep. **160**, 189 (1988).
[11] P. Danielewicz, Nucl. Phys. **A673**, 375 (2000).
[12] Bao-An Li, Phys. Rev. Lett. **85**, 4221 (2000).
[13] J. Aichelin and H. Stöcker, Phys. Lett. **B176**, 14 (1986).
[14] A. Ono, P. Danielewicz, W. A. Friedman, W. G. Lynch, and M. B. Tsang, Phys. Rev. C **68**, 051601(R) (2003).
[15] A. Barrañón, A. Chernomoretz, C. O. Dorso, J. A. López, and J. Morales, Rev. Mex. Fís. **45-Sup. 2**, 110 (1999).
[16] A. Chernomoretz, L. Gingras, Y. Larochelle, L. Beaulieu, R. Roy, C. St-Pierre, and C. O. Dorso, Phys. Rev. C **65**, 054613 (2002).
[17] A. Barrañón, C. O. Dorso, and J. A. López, Rev. Mex. Fís. **47-Sup. 2**, 93 (2001).
[18] A. Barrañón, R. Cárdenas, C. O. Dorso, and J. A. López, Heavy Ion Phys. **17-1**, 59 (2003).
[19] A. Barrañón, C. O. Dorso, and J. A. López, Inf. Tec. **14**, 31 (2003).
[20] A. Barrañón, J. Escamilla, and J. A. López, Phys. Rev. C **69**, 014601 (2004).
[21] A. Barrañón, J. Escamilla, and J. A. López, Braz. J. Phys. **34**, 904 (2004).
[22] R. J. Lenk, T. J. Schlagel, and V. R. Pandharipande, Phys. Rev. C **42**, 372 (1990).
[23] T. L. Hill, J. Chem. Phys. **23**, 617 (1955).
[24] A. Strachan and C. O. Dorso, Phys. Rev. C **56**, 995 (1997).
[25] M. B. Tsang, R. Shomin, O. Bjarki, C. K. Gelbke, G. J. Kunde, R. C. Lemmon, W. G. Lynch, D. Magestro, R. Popescu, A. M. Vandermolen, G. Verde, G. D. Westfall, H. F. Xi, W. A. Friedman, G. Imme, V. Maddalena, C. Nociforo, G. Raciti, G. Riccobene, F. P. Romano, A. Saija, C. Sfienti, S. Fritz, C. Gross, T. Odeh, C. Schwarz, A. Nadasen, D. Sisan, and K. A. G. Rao, Phys. Rev. C **66**, 044618 (2002).
[26] M. B. Tsang, X. D. Liu, L. Shi, P. Danielewicz, C. K. Gelbke, X. D. Liu, W. G. Lynch, W. P. Tan, G. Verde, A. Wagner, H. S. Xu, W. A. Friedman, L. Beaulieu, B. Davin, R. T. de Souza, Y. Larochelle, T. Lefort, R. Yañez, V. Viola, R. J. Charity, and L. G. Sobotka, Phys. Rev. Lett. **92**, 062701 (2004).
[27] M. J. Ison and C. O. Dorso, Phys. Rev. C **71**, 064603 (2005).
[28] C. K. Gelbke *et al*., Phys. Rep. **42**, 311 (1978).
[29] J. López and C. O. Dorso, *Lecture Notes on Phase Transitions in Nuclear Matter* (World Scientific, Singapore, 2000).
[30] A. Dávila, C. Escudero, J. A. López, and C. O. Dorso, submitted to Physica A.